Synthesis of Nanostructured Cr_3C_2-25(Ni20Cr) Coatings

JIANHONG HE, MICHAEL ICE, and ENRIQUE J. LAVERNIA

On the basis of the nanocrystalline Cr_3C_2-25 (Ni20Cr) feedstock powders produced by mechanical milling, a nanostructured coating has been synthesized using high velocity oxygen fuel (HVOF) thermal spraying. The properties of the nanostructured coating were compared to those of the conventional coating of the same composition using scanning electron microscope (SEM), transmission electron microscope (TEM), and microhardness tests. The nanostructured Cr_3C_2-25 (Ni20Cr) coating synthesized in this study had an average carbide particle size of 24 nm. Discontinuous elongated amorphous phases were observed in the nanostructured coating. The conventional Cr_3C_2-25 (Ni20Cr) coatings produced using blended elemental powders exhibited an inhomogeneous microstructure. The observed homogeneity of the nanostructured coating is attributed, in part, to the microstructural improvement of the starting powder. The nanostructured Cr_3C_2-25 (Ni20Cr) coating yielded an average microhardness value of 1020 DPH_{300}, which corresponds to a 20 pct increase in microhardness over that of the conventional coating. The nanostructured Cr_3C_2-25 (Ni20Cr) coating also exhibited a higher apparent fracture toughness relative to that of the conventional coating. The apparent mechanical property improvements in the nanostructured coating were thought to result from the uniformity of the microstructure and the high performance associated with a nanostructured structure. In addition, the mechanism that is present during the milling of a system containing nondeformable particles is discussed in light of the TEM observations.

I. INTRODUCTION

COATINGS based on the WC-Co and Cr_3C_2-NiCr systems are commonly used for wear and corrosion resistant applications. Coatings of the WC-Co system generally have a high hardness and wear resistance. However, the decarburization of WC into W_2C, W_3C, and even metallic W phase leads to the degradation of properties and limits the application of the coatings at temperatures below 450 °C to 530 °C.[1,2] On the other hand, the Cr_3C_2-NiCr system coatings can be used in corrosive environments at service temperatures up to 800 °C to 900 °C.[1–9] Published research shows that the hardness of the Cr_3C_2-NiCr coating slightly decreased only at temperatures below 600 °C and exceeded 600 DPH_{300} at 800 °C.[3] Therefore, Cr_3C_2-NiCr coatings are frequently used as protective coatings for application in corrosive environments at elevated temperatures.[10–14] For instance, erosion of heat-exchange tubes in coal fired and fluidized bed combustion boilers are completely protected by Cr_3C_2-NiCr coatings.[10] These coatings are also used in helium- and sodium- cooled nuclear reactors where H_2, CO, CH_4, and H_2O are potentially contained, and protective oxide films on metal surfaces cannot re-form because of a low oxygen content in the environments; hence, this drastically decreases the protective function provided by typical thermal barrier coatings (MCrAlY).[11–14] However, the main shortcomings of Cr_3C_2-NiCr coatings are low hardness and subsequent low wear resistance compared with WC-Co system coatings.[1] In recent years, thermal spraying using nanostructured feedstock powders has yielded coatings with hardness, strength, and corrosion resistance values higher than the corresponding conventional coatings.[15,16,17] It is therefore anticipated that nanostructured Cr_3C_2-NiCr coatings will possess better performance characteristics. Using mechanical milling, nanostructured Cr_3C_2-NiCr composite powder can be successfully synthesized.[18] This article describes the synthesis and characterization of nanostructured Cr_3C_2-NiCr coatings formed by high velocity oxygen fuel (HVOF) thermal spraying.

JIANHONG HE, Postdoctoral Scientist, MICHAEL ICE, Graduate Student, and ENRIQUE J. LAVERNIA, Professor and Chair, are with the Department of Chemical and Biochemical Engineering and Materials Science, University of California, Irvine, CA 92697-2575.

Manuscript submitted March 30, 1999.

II. EXPERIMENTAL PROCEDURE

A. *Materials*

Nanostructured and conventional Cr_3C_2-NiCr (Dialloy 3004 blended Cr_3C_2-25 (Ni20Cr), with a nominal particle size of $(-45 + 5.5)$ μm, produced by Sulzer Metco Inc. (Westbury, NY) powders were used in the present study. The chemical compositions of the nanostructured and the conventional Cr_3C_2-25 (Ni20Cr) powders are shown in Table I.

The nanostructured powder was synthesized using mechanical milling. The milling process and powder characteristics are described elsewhere.[22] X-ray diffraction and transmission electron microscope (TEM) observations[22] indicated that the as-synthesized nanostructured Cr_3C_2-25 (Ni20Cr) powder consisted of mainly Cr_3C_2, some Cr_7C_3, and NiCr solid solution. This is the same phase constituent as the conventional powder.[6] The average grain size of the nanostructured powder was 15 nm.

B. *Agglomeration*

The thermal spray process typically requires a powder size within the range of 10 to 50 μm. The as-synthesized nanostructured Cr_3C_2-25 (Ni20Cr) powder is approximately 5 μm and, hence, not suitable for thermal spraying in this condition because the HVOF requires a particle size of 10 to 50 μm. Accordingly, a procedure was established for the

Table I. Chemical Composition of Cr_3C_2-25 (Ni20Cr) Powders (Weight Percent)

Powder Type	Cr	Ni	C	N	O
Conventional powder	70.0	19.2	9.83	0.20	0.21
Nanostructured powder	64.3	18.8	9.36	0.51	1.93

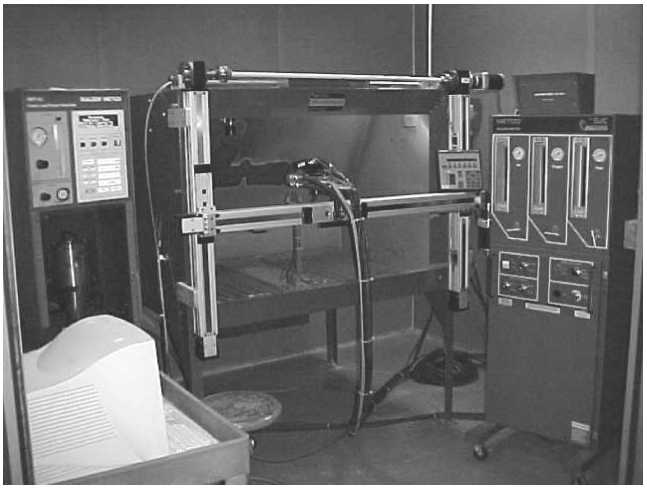

(*a*)

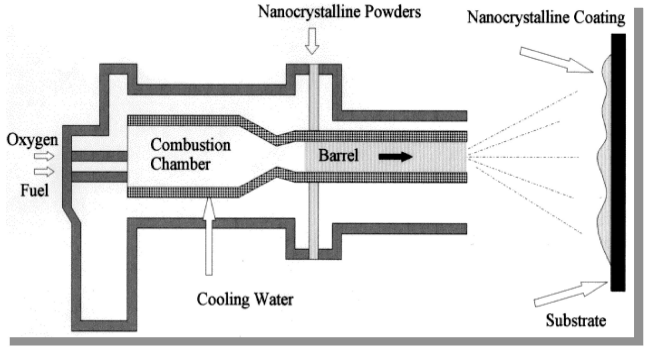

(*b*)

Fig. 1—HVOF process for Cr_3C_2-25(Ni20Cr) coatings: (*a*) HVOF thermal spray facility and (*b*) schematic of HVOF process.[16]

agglomeration of the Cr_3C_2-25 (Ni20Cr) powder into larger-sized particles. Using a 2 pct methyl cellulose solution in H_2O, the powder is made into a slurry. This slurry was annealed in a vacuum furnace at a temperature of 80 °C for a time period ranging from 24 to 48 hours. The annealing time is a function of the quantity of the slurry to be baked. As a result of the annealing, a solid block of material was formed. This block is relatively brittle and can easily be crushed into powder. This powder was then sieved through a sub-50 μm mesh. The resulting powder was found to have an adequate particle size (approximately 40 μm) to flow in the HVOF system used.

C. *HVOF Thermal Spray Process*

To spray the Cr_3C_2-25(Ni20Cr) coatings, a Sulzer Metco Diamond Jet HVOF thermal spray facility, which is shown in Figure 1(a), was used. The main constituents of this facility are a DJC control unit, a 9-MP powder hopper feeder, a "Parker" X-Y automated traverse unit, "In-Flight" diagnostic equipment, and the Diamond Jet spray gun. The DJC control unit monitors and controls the gas flow into the gun and allows the proper stoichiometric ratios to be set for optimum spray performance. The 9-MP powder feeder is a fluidized bed powder feed unit that allows proper control of the powder flow into the gun. To obtain repeatable results, a "Parker" automated X-Y system was installed to aid in producing a predictable, uniform coating thickness because the substrate is uniformly scanned by the X-Y traverse controlled gun, and the coating thickness produced by each scan is calculable. With the "In-Flight" diagnostic equipment, accurate average particle temperatures can be measured as well as trajectory and particle flow characteristics. The Diamond Jet spray gun is a hybrid water-cooled gun that allows easy transitions between the two possible fuel gases, hydrogen and propylene.

As shown in Figure 1(b), the Diamond Jet brings in oxygen, air, and fuel, in this experiment propylene, from the DJC into the rear of the gun in the proper stoichiometric ratios. This gaseous mixture is ignited by an arc current creating a hypersonic, low temperature flame with gas velocities of 1830 m/s and temperatures around 2700 K. From the 9-MP hopper powder feed unit, nitrogen carrier gas brings the agglomerated powder into the rear of the gun and then axially into the flame. The powder is heated in the gun barrel then sprayed out onto a stainless steel substrate. The spraying parameters are summarized in Table II.

D. *Coating Characterization*

The cross section of the coating was examined using a PHILIPS* XL 30 FEG scanning electron microscope (SEM).

*PHILIPS is a trademark of Philips Electronic Instruments Corp., Mahwah, NJ.

The microhardness was tested on a Buehler Micromet 2004 Microhardness tester using a load of 300 g. Each microhardness value was obtained from an average value of 30 tests. After removal of the substrate by polishing, the TEM specimens were prepared by cutting out a section of the coating and forming 3-mm-diameter disks. The disks were dimpled to around 30-μm thick using a dimpler fitted with diamond grinders. The grinding size descended from 6-μm grade, down to 3 μm, and finally to 1-μm grade. The final thinning perforation process was performed using an argon ion miller. With the prepared samples, TEM observations were carried out on the PHILIPS CM20 microscope operated at 200 keV.

III. RESULTS AND DISCUSSION

A. *Synthesis of Nanostructured Composite*

Mechanical milling is an effective process for the synthesis of nanostructured powders[18,19,20] because the powder grains are continuously refined by the cold welding and fracturing process.[21] Nanostructured composites consisting of hard particles with a metal binder, such as Cr_3C_2-25 (Ni20Cr) and WC-12Co systems, have been successfully synthesized using mechanical milling.[22,23] During milling, small amounts of powder samples (< 10 g) were removed from the vessel every 2 hours. These samples were examined using X-ray diffraction, SEM, and TEM. On the basis of the

Table II. Spraying Parameters Used to Produce Cr_3C_2-25(Ni20Cr) Coatings

Gas	Pressure (MPa)	FMR*	GSF**	Parameter	Setting
Air	0.69	48	6740	powder feed rate	0.315 g/s
Fuel	0.69	40	1384	X-Y traverse speed	1.016/s
Nitrogen	1.034	55	220	spraying distance	0.230 m
Oxygen	1.034	40	4546	—	—

*FMR: flow meter reading.
**GSF: gas standard flow (mm^3/s).

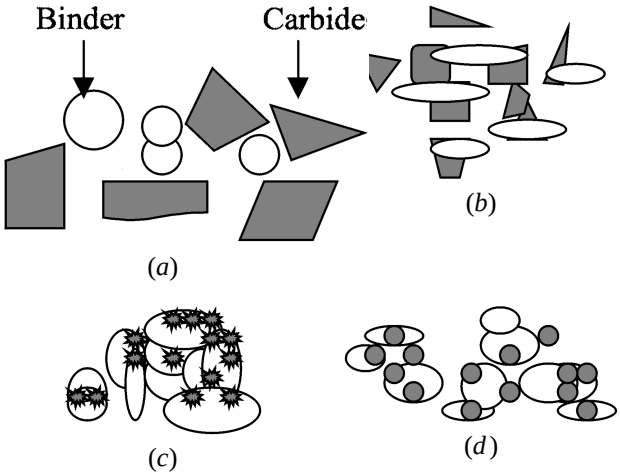

Fig. 2—(*a*) through (*d*) Schematic of milling mechanism for duplex structure powder.

structure, morphology, and dimension analysis, the milling mechanism of a duplex structure powder (hard particles with metal binder) is schematically illustrated in Figure 2. Hard and brittle carbides are first fractured into sharp fragments and embedded into the metal binder. Then the metal binder, with lower hardness, is subjected to enhanced milling from both the milling media (in the present case, stainless steel balls) and hard carbide particles. As milling time increases, carbide fragments are continually embedded into the metal binder. The metal binder and the polycrystal composite experience continuous overlapping, cold welding, and fracturing. With time, sharp carbide fragments in the polycrystal composite are shaped into round particles. Finally, a polycrystal nanocomposite powder system, in which round nanosize carbide particles are uniformly distributed in a metal binder, is formed. As an example, Figures 3(a) and (b) shows a TEM bright-field and the corresponding dark-field image of a Cr_3C_2-25 (Ni20Cr) polycrystal nanocomposite powder. Clearly shown are large proportions of carbides, in the form of round particles, uniformly distributing themselves in the NiCr solid solution.

In addition to the Cr_3C_2-NiCr and WC-Co systems, it is possible to use mechanical milling to synthesize nanocomposite powder systems with a hard particle and tough binder duplex structure; examples of such systems are WC-NiCr, TiC-NiCr, TiC-Ti, and SiC-Al.

B. *Microstructure of Coatings*

The synthesized nanocomposite powder was agglomerated to a size ranging from 10 to 50 μm before HVOF

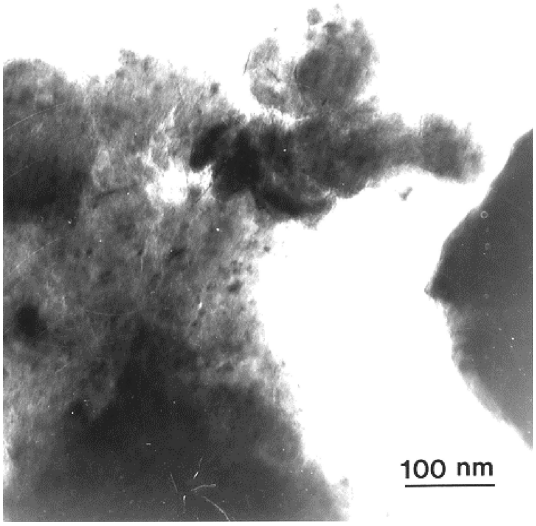

(*a*)

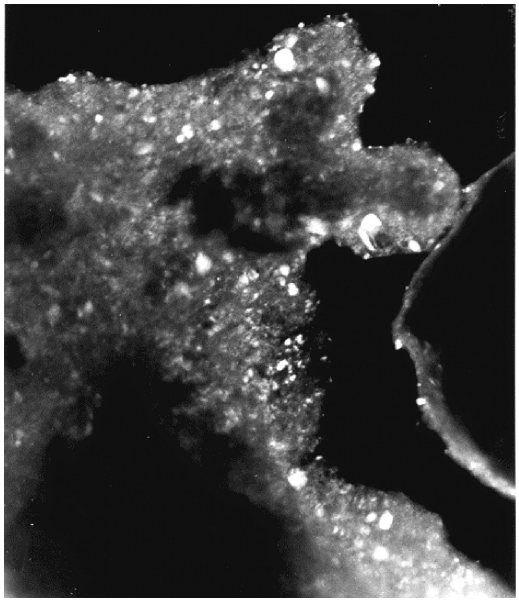

(*b*)

Fig. 3—Cr_3C_2-25(Ni20Cr) polycrystal nanocomposite powder: (*a*) bright-field image; and (*b*) corresponding dark-field image, using (121) reflection of Cr_3C_2 carbide.

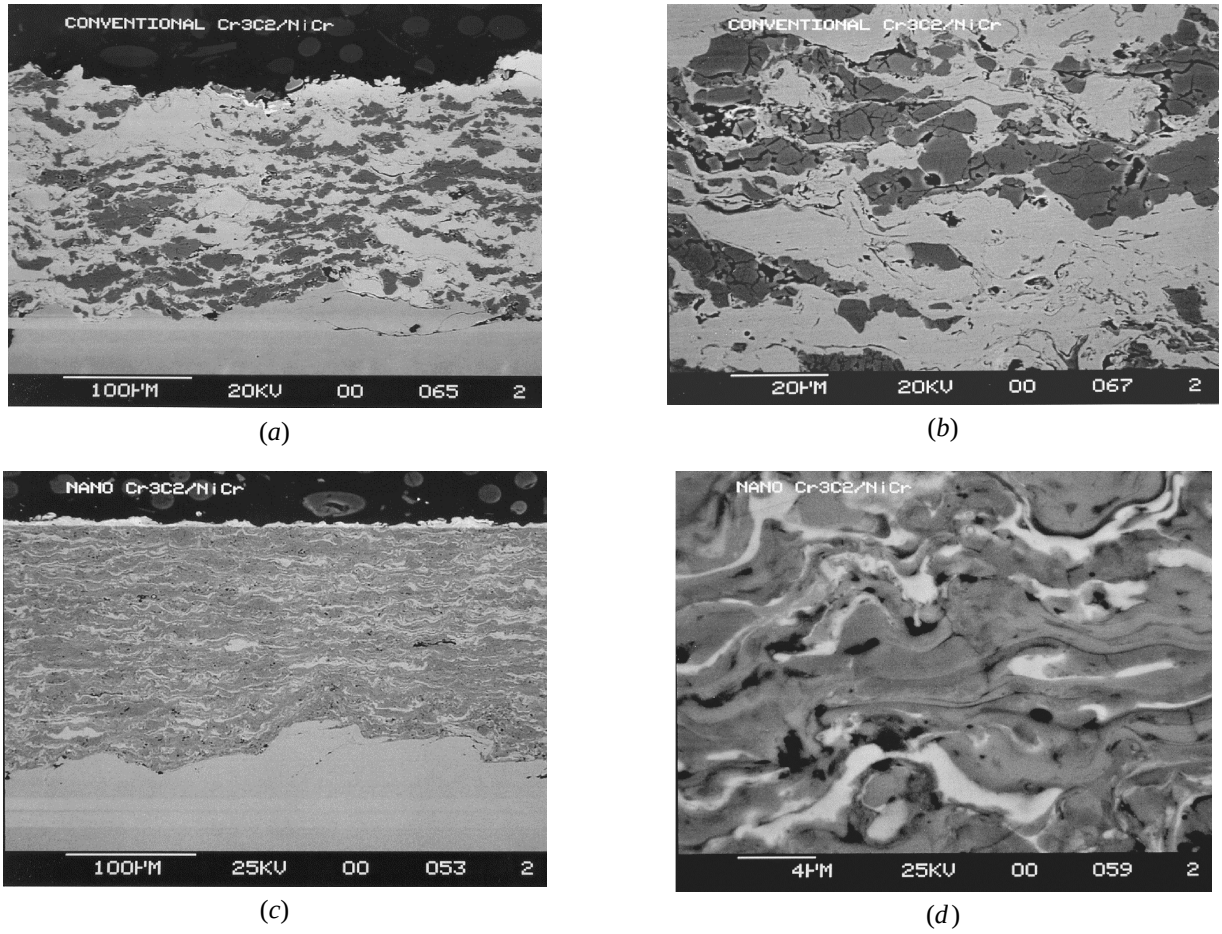

Fig. 4—Microstructure of Cr_3C_2-25(Ni20Cr) coatings. (*a*) conventional coating, (*b*) magnification of (a), (*c*) nanostructured coating, and (*d*) magnification of (c).

thermal spraying; the procedure employed was described in section II-B. The microstructures of conventional and nanostructured Cr_3C_2-25 (Ni20Cr) coatings, examined using SEM, are shown in Figure 4. A uniform and dense microstructure is observed in the nanostructured coatings, compared to the conventional Cr_3C_2-25 (Ni20Cr) coatings that are observed to have an inhomogeneous microstructure. Five of each dark and bright areas were randomly chosen for SEM EDS analysis of their chemical composition. The results of this analysis are listed in Table III. The distributions of Cr and Ni in dark and bright areas were obtained from the average value of five readings. The row labeled average in Table III was obtained from low magnification analysis (a number of dark and bright areas were in the field of view) and was also the average value of five readings.

Table III. Chemical Composition of Cr_3C_2-25(Ni20Cr) Coatings (Weight Percent)

	Conventional Coating		Nanostructured Coating	
Area	Cr	Ni	Cr	Ni
Average	46.3	53.7	76.25	23.75
Bright area	16.21	83.79	31.12	68.88
Dark area	99.15	0.85	94.34	5.66

A comparison of EDS peaks from Ni and Cr in both bright and dark areas is shown in Figure 5. In the bright area of the conventional coating, the contents of Cr and Ni are close to the nominal chemical composition of pure NiCr solid solution (80 pct Ni and 20 pct Cr), thus, the bright area is considered to be the NiCr solid solution binder phase. A Ni peak is not observed in the dark area (Figure 5), although a minor amount of Ni exists (0.85 pct), thus, the dark area is considered to be the carbide phase. For the nanostructured coating, a higher Cr content in the bright area and a higher Ni content in the dark area are observed. On the basis of the considerations discussed subsequently, in the nanostructured coatings, the bright area is still considered as the NiCr binder phase, whereas the dark area is a nanocomposite consisting of carbide particles and a NiCr binder phase. An explanation of the structure is as follows. During milling, carbide particles were fractured and embedded into the binder phase. Thus, most of the binder phase is combined with fractured carbide particles to form a nanocomposite, leaving a small amount of the binder phase feedstock powder. However, the binder phase was not a completely pure NiCr solid solution, it contained some carbide particles. This caused a higher Cr content in the binder phase in the nanostructured coating. Similarly, the binder phase was present in the gaps between fractured carbide particles in the nanocomposite feedstock powder, giving the result that Ni is observed in the carbide

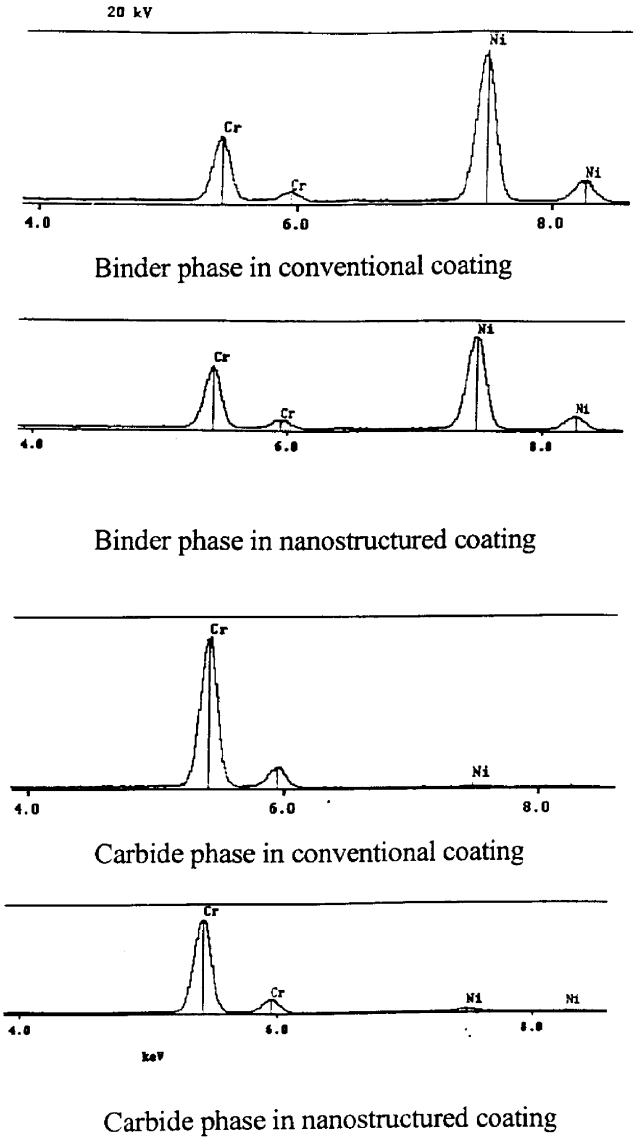

Fig. 5—EDS peaks from Ni and Cr elements in individual phase in conventional and nanostructured coatings.

phase of the nanostructured coating. Also, the measurement of elements in individual phases of the nanostructured coating is partly affected by the beam size limitations of the EDS. Because both the binder and carbide phases are extremely fine in the nanostructured coating, a pure binder phase area or carbide phase area cannot be perfectly isolated for SEM EDS analysis. Thus, the constituents of the binder phase in the nanostructured coating likely include a carbide phase or *vice versa*.

To compare the average chemical composition (labeled average in Table III) of the coatings with those of the feedstock powders listed in Table I, a simple correction for data in Table III was made because the light elements, such as C, N, and O, were not included in the EDS analysis. In Table III, the sum of Cr and Ni content is 100 pct. Actually, the sum of Cr and Ni content is 89.2 pct in the conventional feedstock powder and 83.1 pct in the nanocomposite feedstock powder (Table I). Therefore, the content of Cr and Ni is multiplied by factors of 0.892 in the conventional coating and 0.831 in the nanostructured coating. This correction represents a simple approximation because it implies that there were no changes in the contents of all elements during thermal spraying, whereas in practice, this may not be the case. After making this simple correction, the average contents of Cr and Ni are 41.3 pct and 47.9 pct in the conventional coating and 63.4 and 19.8 pct in the nanostructured coating, respectively. It is worth noting that there is a large average chemical composition difference between the conventional and nanostructured coatings. The average contents of Cr and Ni in the nanostructured coatings are close to those of feedstock nanocomposite powder. However, those same values found for the conventional coating differ markedly from the conventional feedstock powder. Because the contents of Ni and Cr in both the binder and the carbide phase are close to their nominal contents, the chemical composition difference between the conventional coating and feedstock powder is attributed to a decrease in the volume fraction of the carbide phase in the conventional coating. In related studies, the decarburization of tungsten carbide is widely reported,[1,2] whereas chromium carbide is quite stable during thermal spraying.[6] Therefore, the measured decrease in the volume fraction of the carbide phase in the conventional coating may not be attributed to decarburization or oxidation of chromium carbide. It is known[22] that individual, large irregularly shaped carbide particles and spherically shaped binder phase particles are present in blended Cr_3C_2-25 (Ni20Cr) powder. During spraying, the large carbide particles, with a high melting point of 2200 K (T_l), may remain solid or semi-molten in the HVOF system (short dwell time and low temperature flame), yielding low adherence with the substrate surface. Conversely, melted binder phase droplets (melting point is 1690 K) have a more fluid characteristic than the carbide particles. This greater fluidity can result in the effective contact of the binder phase with the substrate surface. Thus, the volume fraction of the carbide phase decreases in the conventional coatings as a fraction of the carbide particles fail to adhere and simply bounce off the substrate. In the case of the nanocomposite feedstock powder, there is a high probability that the nanoscale carbide particles will be completely surrounded by the binder phase as a result of their extremely small size (15 nm). The nanoscale particles are therefore wetted by the binder phase and effectively adhere to the substrate surface. This improved fluidity leads the nanostructured coating to maintain a close composition with the feedstock powder. Current efforts are aimed at providing quantitative support to this suggestion *via* studies of carbide particle size distribution during milling.

The commercially available blended Cr_3C_2-NiCr powders are mixtures of Cr_3C_2 and NiCr solid solution, and these mixtures are inherently difficult to handle because of their segregation during storage, transportation, and spraying.[8,24] Consequently, these mixtures usually produce inhomogeneous microstructure characteristics.[8,24] In this study, the decrease in the volume fraction of the carbide phase in the conventional coating was indicative of nonuniformity in the microstructure. Coating performance is known to be very susceptible to the nonuniformity of the microstructure.[3,8,24] A few pretreatment methods have been developed to overcome these types of microstructural variations. Two such

methods, referred to as "prealloying"[24] and "cladding,"[8] are widely used. Using the prealloying method, the powders are first agglomerated using an organic polymeric binder and then heated and presintered in hydrogen. The powders are then densified using a plasma flame in an inert atmosphere and are finally milled, screened, and classified to yield the desired particle size. In a related study,[24] the hardness of a plasma-sprayed Cr_3C_2-25 (Ni20Cr) coating, using the prealloyed powder, increased from 594 to 796 DPH_{300}. In the cladding method, each Cr_3C_2 carbide particle is clad with an essentially continuous layer of NiCr solid solution; therefore, the Cr_3C_2 carbide is present as a discrete second phase particle randomly embedded in a NiCr solid solution. In related work,[8] the hardness of a plasma-sprayed Cr_3C_2-50 (Ni20Cr) coating increased from 620 to 860 DPH_{300}, and the wear resistance was also improved as compared to the standard blend coating method, presumably as a result of the uniform "clad" powder.[8] Using a Metco Diamond Jet system, Sasaki *et al.*[3] compared the behavior of HVOF thermally sprayed coatings made using four different types of Cr_3C_2-25 (Ni20Cr) feedstock powders (blend, agglomerated/sintered, sintered/crushed, and sintered/crushed/clad). They found that the coatings made from the sintered/crushed/clad powder showed the best characteristics as compared to those coatings sprayed by the other three types of powders. Therefore, regardless of the spraying method employed, the uniformity of microstructure in a coating has a significant positive influence on its performance.

In the present study, the Cr_3C_2-NiCr nanocomposite powder is synthesized using mechanical milling and agglomeration. In this approach, the carbides in the nanocomposite powder are uniformly distributed in the NiCr solid solution. In essence, our approach yields a clad powder, and, hence, a uniform microstructure is obtained in the nanostructured coating. In other words, the synthesis method of nanocomposite feedstock powder used in the present study provides a beneficial role in the uniformity of the coating microstructure.

The TEM bright-field image of the nanostructured coating, the corresponding dark-field image, and diffraction pattern are shown in Figures 6(a) and (c), respectively. The average carbide particle size is approximately 24 nm. This indicates that the coating has a nanostructured microstructure. In a nanostructured WC-12 pct Co coating,[23] TEM examination revealed a microstructure consisting of nanosized WC carbide particles in an amorphous matrix phase. While in the nanostructured Cr_3C_2-NiCr coatings, the diffraction pattern shown in Figure 6(c) does not exhibit clearly the presence of an amorphous matrix phase. Guilemany and Calero[6] also observed amorphous matrix phases in a conventional HVOF thermally sprayed Cr_3C_2-NiCr coating. Instead of an amorphous matrix phase, a few discontinuous elongated amorphous phases are observed in the nanostructured Cr_3C_2-NiCr coating, as shown in Figures 7(a) through (d). The inserted diffraction patterns, which were from the elongated phases marked *A*, show diffuse rings. Many fine diffraction spots are sharply imaged in the diffraction patterns; this indicates that the diffraction patterns are well focused. The diffuse rings are thus indicative of an amorphous phase rather than a false appearance caused by under/over focusing. These elongated amorphous phases, which have dimensions of around 100-nm wide and 1-μm long, are discontinuously distributed in the coating.

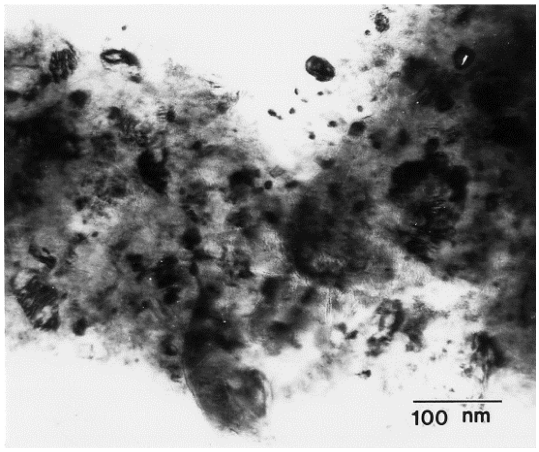

(*a*)

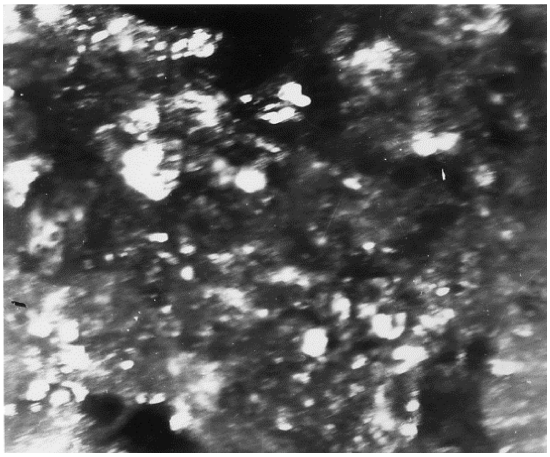

(*b*)

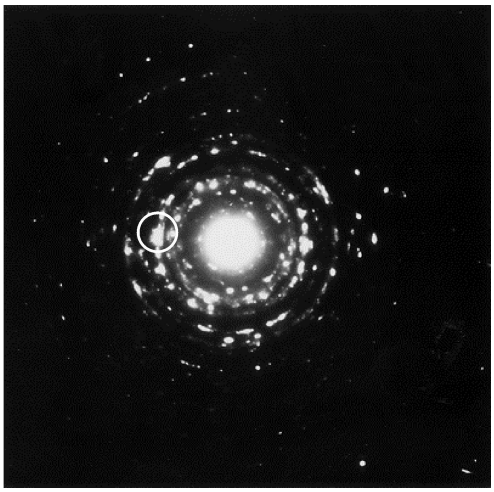

(*c*)

Fig. 6—TEM observation of nanostructured Cr_3C_2-25(Ni20Cr) coating: (*a*) bright-field image, (*b*) dark-field image using (121) reflection of Cr_3C_2 carbide shown by a white circle in (c), and (*c*) corresponding diffraction pattern.

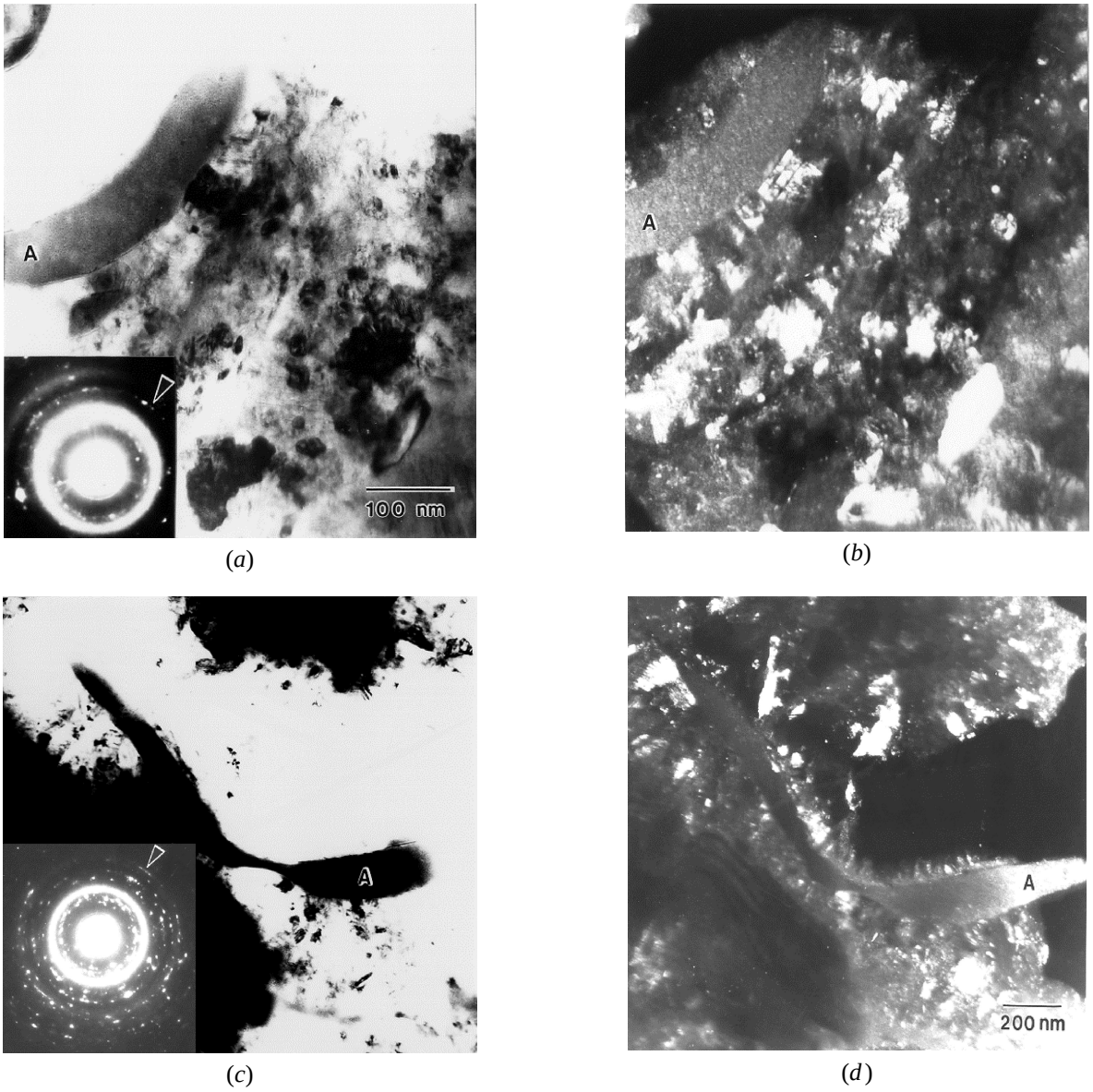

Fig. 7—Elongated amorphous phase in nanostructured Cr_3C_2-25(Ni20Cr) coating: (*a*) bright-field image, (*b*) dark-field image, (*c*) bright-field image, and (*d*) dark-field image.

C. *Microhardness*

The average microhardness of the nanostructured Cr_3C_2-25(Ni20Cr) coating, taken on the cross section, increases from a value of 846 for the conventional Cr_3C_2-25(Ni20Cr) coating to 1020 DPH_{300} for the nanostructured coating. Hence, the nanostructured coating exhibits to a 20.5 pct increase in microhardness as compared with the corresponding conventional coating. Several published hardness values of Cr_3C_2-25(Ni20Cr) coatings are listed in Table IV.

The spraying methodology and the type of feedstock powder used (blend, agglomeration, or clad) have a very significant influence on the hardness of coatings on the basis of the data in Table IV. Effects of the spraying method[7,26] and type of feedstock powder[2,3,8,24] on hardness has been extensively investigated. High velocity oxygen fuel is characterized by high particle velocity and low thermal energy; this combination of high kinetic energy and low thermal energy leads to a high hardness.[1] The clad feedstock powders produce uniform Cr_3C_2-NiCr coatings and, hence, high hardness.[3,8] It has been reported that the hardness of nanostructured materials often exhibits a two- to fivefold increase compared to that of the corresponding conventional materials, although it is lower than that predicted using the classical Hall–Petch equation.[27,28,29] In a related study, Kear and McCandlish[15] also indicated that nanostructured WC-23 pct Co coatings have a higher hardness than that of the conventional coating of the same composition. Therefore, the high hardness of the nanostructured Cr_3C_2-25 (Ni20Cr) coatings results primarily from two aspects: (1) uniformity of microstructure, caused by the synthesis process of nanocomposite feedstock powder; and (2) the intrinsically high hardness of nanostructured materials.

The abrasion resistance of thermal sprayed coatings is significantly related to the relative fracture toughness.[30]

Table IV. Published Hardness Data of Cr_3C_2-25 (Ni20Cr) Coatings

Spraying method	Powder	Hardness	Reference
HVOF	commercial	855 (HV_{300})	25
HVOF	commercial (sintered/crushed/clad)	950 (DPH_{300})	3
HVOF	commercial (blend)	700 (DPH_{300})	3
HVOF	commercial (agglomeration)	914 (DPH_{300})	2
HVOF	commercial (blend)	697 (DPH_{300})	2
Detonation gun spraying	commercial: powder size: 10 to 44 μm	800 (HV_{300})	10
Atmospheric plasma spraying, Ar/H_2	commercial	830 (HV_{300})	7
Atmospheric plasma spraying, Ar/He	commercial	871 (HV_{300})	7
HVOF (Hobart Tafa Technologies JP-5000 HP)	commercial	1033 (HV_{300})	7
Continuous detonation spraying	commercial	828 (HV_{300})	7
Atmospheric plasma spraying, Ar/H_2	commercial	837 (HV_{300})	26
Atmospheric plasma spraying, Ar/He	commercial	943 (HV_{300})	26
Continuous detonation spraying	commercial	889 (HV_{300})	26
Detonation gun spraying	commercial	945 (HV_{300})	26
HVOF	commercial (blend)	846 (DPH_{300})	this study
HVOF	nanostructured	1020 (DPH_{300})	this study

The indentation fracture method is often employed to characterize the relative fracture toughness of the coatings.[30] In this study, an indentation fracture examination was performed, and the results are shown in Figures 8(a) through (d). Under the same load, indentation marks in the nanostructured coating are smaller than those in the conventional coating because the nanostructured coating has a higher hardness. Under a load of 1000 g, many cracks caused by an indentation along the phase interface of the carbide phase with the metal binder phase are observed in the conventional coating, and some cracks are also found in the nanostructured coating. In sintered hardmetal cements,[31] four symmetrical indentation cracks were observed on the extended lines of the diagonals related to the quadrilateral pyramid indentation where a maximum stress concentration caused by indentation is present. Whereas, in the present coatings, indentation cracks usually appear in the direction parallel to the coating surface, however, they are not present directly on the extended line of the diagonal of the indentation. No cracks are observed in the direction perpendicular to the coating surface. These results show the following. (1) Crack propagation within the coatings has a favored direction, and higher resistance to indentation fracture is present in the direction perpendicular to the coating surface. The presence of a preferred direction for crack propagation is attributed to the thermal spray process. A complete coating was gradually produced by passing the thermal spray torch across the substrate 15 times. Each pass formed a coating layer approximately 15-μm thick. Because each layer had once been outer surface, there was a potential for contamination to occur and become covered by the next layer. Moreover, at layer boundaries, discontinuity in heat and mass transfer may have led to a discontinuity in the behavior of the coating. (2) The interface formed between carbide and metal binder is a preferred site for crack propagation because there is a significant difference in the physical properties, *i.e.*, thermal expansion coefficient, between the carbide phase and metal binder phase.

When the load was decreased to 500 g, a few cracks around the indentation are still observed in the conventional coating, whereas none are present the nanostructured coating. These results suggest that the nanostructured Cr_3C_2-25 (Ni20Cr) coating possesses a higher apparent fracture toughness relative to that of the conventional material. Further work in this area is continuing in an effort to provide more insight into the fracture behavior of nanostructured coatings.

IV. CONCLUSIONS

A nanostructured Cr_3C_2-25 (Ni20Cr) coating was synthesized using mechanical milling and HVOF thermal spraying. The characteristics of the nanostructured and the corresponding conventional coatings were investigated using SEM, TEM, and microhardness tests. Results obtained are summarized as follows:

1. The milling mechanisms of the powder system consisting of hard particles in a tough matrix were summarized.
2. The average carbide particle size decreased from approximately 20 μm in the conventional Cr_3C_2-25 (Ni20Cr) coating to 24 nm in the nanostructured coating synthesized in this study. A few discontinuous elongated amorphous phases were observed in the nanostructured coating.
3. The conventional Cr_3C_2-25 (Ni20Cr) coating, made of blended powder, revealed an inhomogeneous microstructure, whereas a uniform microstructure was observed in the nanostructured Cr_3C_2-25 (Ni20Cr) coating. This was attributed to the individual synthesis process.
4. The microhardness increased from 846 for the conventional Cr_3C_2-25 (Ni20Cr) coating to 1020 DPH_{300} for the nanostructured coating. Based on simple indentation measurements, the nanostructured Cr_3C_2-25 (Ni20Cr) coating also had a higher apparent fracture toughness relative to that of the conventional material. This improvement in the characteristics of the coatings was attributed to the uniformity of microstructure within the nanostructured coating and the intrinsically high performance of nanostructured materials.

ACKNOWLEDGMENTS

The authors gratefully acknowledge financial support provided by the Office of Naval Research (Grant Nos.: N00014-94-1-0017, N00014-97-1-0844, and N00014-98-1-0569).

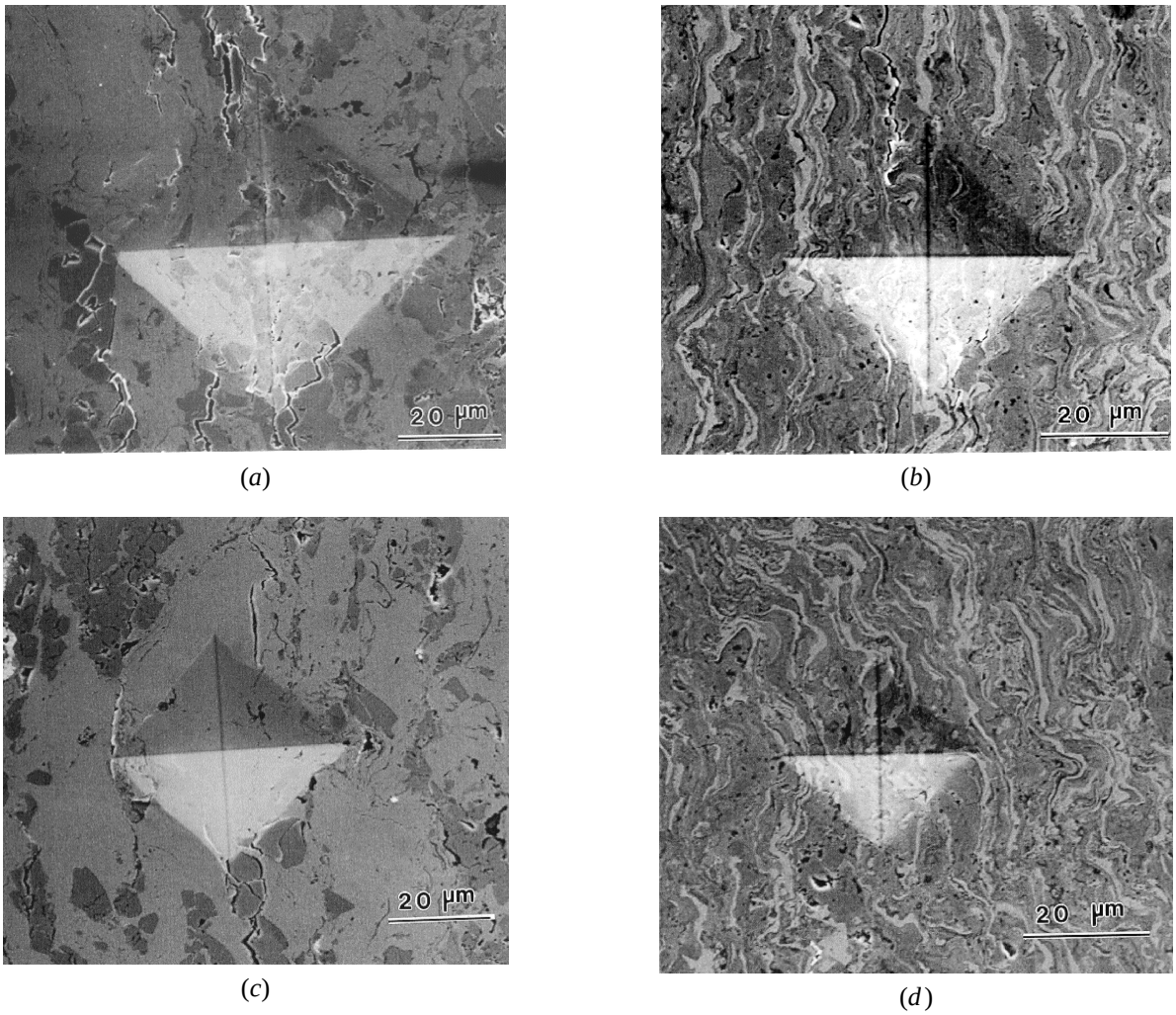

(*a*) (*b*) (*c*) (*d*)

Fig. 8—Indentation cracking. Micrographs are orientated such that the coating surface is in the vertical direction on the paper. (*a*) Conventional coating at 1000 g; (*b*) nanostructured coating at 1000 g; and (*c*) conventional coating at 500 g; (*d*) nanostructured coating at 500 g.

REFERENCES

1. P. Vuoristo, K. Niemi, T. Mantyla, L.M. Berger, and M. Nebelung: in *Thermal Spray Science & Technology*, C.C. Berndt and S. Sampath, eds., ASM INTERNATIONAL, Materials Park, OH 1995, pp. 309-15.
2. L. Russo and M. Dorfmann: in *Thermal Spraying: Current Status and Future Trends*, A. Ohmori, ed., High Temperature Society of Japan, Osaka, Japan, 1995, pp. 681-86.
3. M. Sasaki, F. Kawakami, C. Komaki, and M. Ishida: in *Thermal Spray: International Advances in Coatings Technology*, C.C. Berndt, ed., ASM INTERNATIONAL, Materials Park, OH, 1992, pp. 165-70.
4. E. Lugscheider, P. Remer, C. Herbst, K. Yushchenko, Y. Borisov, A. Chernishov, P. Vitiaz, A. Verstak, B. Wielage, and S. Steinhauser: in *Thermal Spraying: Current Status and Future Trends*, A. Ohmori, ed., High Temperature Society of Japan, Osaka, Japan, 1995, pp. 235-40.
5. S.Y. Hwang and B.G. Seong: in *Thermal Spray Coatings: Research, Design and Applications*, C.C. Berndt and T.F. Bernecki, eds., ASM INTERNATIONAL, Materials Park, OH, 1993 pp. 587-92.
6. J.M. Guilemany and J.A. Calero: in *Thermal Spray: A United Forum for Scientific and Technological Advances*, C.C. Berndt, ed., ASM INTERNATIONAL, Materials Park, OH, 1997, pp. 717-21.
7. P. Vuoristo, K. Niemi, A. Makela, and T. Mantyla: in *Thermal Spray Industrial Applications*, C.C. Berndt and S. Sampath, eds., ASM INTERNATIONAL, Materials Park, OH, 1994, pp. 121-26.
8. J.D. Reardon, R. Mignogna, and F.N. Longo: *Thin Solid Films*, 1981, vol. 83, pp. 345-51.
9. O. Knotek, R. Elsing, and H.R. Heintz: *J. Vac. Sci. Technol.*, 1985, vol. A3, pp. 2490-93.
10. Y. Fukuda and M. Kumon: in *Thermal Spraying: Current Status and Future Trends*, A. Ohmori, ed., High Temperature Society of Japan, Osaka, Japan, 1995, pp. 107-11.
11. G.Y. Lai: *Thin Solid Films*, 1978, vol. 53, pp. 343-51.
12. G.Y. Lai: *Thin Solid Films*, 1979, vol. 64, pp. 271-80.
13. C.C. Li: *Thin Solid Films*, 1980, vol. 73, pp. 59-77.
14. T.A. Taylor, M.P. Overs, J.M. Quets, and R.C. Tucker, Jr: *Thin Solid Films*, 1983, vol. 107, pp. 427-35.
15. B.H. Kear and L.E. McCandlish: *Nanostr. Mater.*, 1993, vol. 3, pp. 19-30.
16. M.L. Lau, H.G. Jiang, W. Nuchter, and E.J. Lavernia: *Phys. Status Solidi (a)*, 1998, vol. 166, pp. 257-68.
17. E.J. Lavernia, M.L. Lau, and H.G. Jiang: in *Thermal Spray Processing of Nanocrystalline Materials, Nanostructured Materials*, G.M. Chow and N.I. Noskova, eds., Kluwer Academic Publishers, Hingham, MA, 1998, pp. 283-302.
18. H. Gleiter: *Deformation of Polycrystals: Mechanisms and Microstructures*, Proc. 2nd Ris Symp., Roskilde, Denmark, H. Hansen, A. Horsewell, T. Laffer, and A. Lilholt, eds., Riso National Laboratory, Roskilde, Denmark, 1981, p. 15.
19. R. Sundaresen and F.H. Froes: *J. Met.*, 1987, vol. 39, p. 22.
20. C.C. Koch: in *Mechanical Alloying*, P.H. Shingu, ed., Trans Tech Publications, Aedermannsdorf, *Mater. Sci. Forum*, 1992, vols. 88–90, pp. 243-62.
21. J.S. Benjamin: in *Mechanical Alloying*, P.H. Shingu, ed., Trans Tech Publications, Aedermannsdorf, 1992; *Mater. Sci. Forum*, 1992, vols. 88–90, pp. 1-18.
22. J. He, M. Ice, and E.J. Lavernia: *NanoStr. Mater.*, 1998, vol. 10, pp. 1271-83.

23. J. He, M. Ice, S. Dallek, and E.J. Lavernia: *Metall. Mater. Trans. A*, 2000, vol. 31A, pp. 541-53.
24. D.L. Houck and R.F. Chency: *Thin Solid Films*, 1984, vol. 118, pp. 507-13.
25. D.C. Crawmer, J.D. Krebsbach, and W.L. Riggs: in *Thermal Spray: International Advances in Coatings Technology*, C.C. Berndt, ed., ASM INTERNATIONAL, Materials Park, OH, 1992, pp. 127-36.
26. K. Niemi, P. Vuoristo, T. Mantyla, G. Barbezat, and A.R. Nicoll: in *Thermal Spray: International Advances in Coatings Technology*, C.C. Berndt, ed., ASM INTERNATIONAL, Materials Park, OH, 1992, pp. 685-89.
27. X.D. Liu, M. Nagumo, and M. Umemoto: *Mater. Trans., JIM*, 1997, vol. 38, pp. 1033-39.
28. C. Suryanarayana, D. Mukhopadhyay, S.N. Patankar, and F.H. Froes: *J. Mater. Res.*, 1992, vol. 7, pp. 2114-17.
29. D.A. Konstantinidis and E.C. Aifantis: *NanoStruct. Mater.*, 1998, vol. 10, pp. 1111-18.
30. S. Usmani, S. Sampath, and H. Herman: in *Thermal Spray Processing of Nanoscale Materials—A Conference Report with Extended Abstracts*, C.C. Berndt and E.J. Lavernia, eds.; *J. Thermal Spray Technol.*, 1998, vol. 7, pp. 429-31.
31. K. Jia, T.E. Fischer, and B. Gallois: *NanoStr. Mater.*, 1998, vol. 10, pp. 857-91.